

Increased Amino Acid Transport into Brain Tumors Measured by PET of L-(2-¹⁸F)Fluorotyrosine

K. Wienhard, K. Herholz, H. H. Coenen, J. Rudolf, P. Kling, G. Stöcklin, and W.-D. Heiss

Max-Planck-Institut für neurologische Forschung, Köln, Germany and Institut für Chemie I (Nuklearchemie) der Kernforschungsanlage, Jülich, Germany

The uptake of L-(2-¹⁸F)fluorotyrosine (F-Tyr), a newly synthesized amino acid tracer, was studied in 15 patients with various brain tumors by dynamic PET. The higher F-Tyr accumulation in tumors (mean 27% above contralateral tissue) was associated with two-fold transport rates into tumors, while the rate constants describing irreversible incorporation were decreased. The increased F-Tyr transport was not correlated to ⁶⁸Ga-EDTA accumulation and cannot be explained by disruption of the blood-brain barrier. Kinetic analysis of 2-(¹⁸F)-fluoro-deoxy-glucose accumulation in the same patients demonstrated that increased metabolic rates in tumors are mainly caused by altered phosphorylation rates while transport of glucose is less affected. Since F-Tyr transport rates clearly separated tumors from normal tissue and since F-Tyr accumulation was related to tumor grade, PET studies of F-Tyr uptake are of clinical value for diagnosis and classification of brain tumors.

J Nucl Med 1991; 32:1338-1346

The estimation of local cerebral protein synthesis rates in man by positron emission tomography (PET) of the accumulation of labeled amino acids is limited since incorporation rates into proteins and metabolic pathways are different for various amino acids and metabolites as well as competing substrates for t-RNA cannot be quantified in the usual clinical setting. Therefore, variables and constants defining applicable kinetic models cannot be described with sufficient accuracy to provide reliable measurements of in vivo protein synthesis. While quantitation of the incorporation rates of various amino acids into proteins and of their alterations would help to understand processes of development, learning and memory, and to describe molecular mechanisms of defined enzymatically linked diseases, a less specific assessment of local accumulation of amino acids could provide insight into pathophysiological mechanisms involved in neuronal damage, cell

regeneration, degenerative diseases, and neoplasias (1). Since imaging modalities alone do not provide data suited for inter- and intra-individual comparisons, measured parameters of kinetic models of tracer accumulation might be helpful in differentiating between normal and pathologic tissue.

Most amino acids used for PET applications so far have been labeled with ¹¹C (2-7), which limits their use in the assessment of the rather slow incorporation into proteins by the short half-life of this positron emitter. The recently synthesized L(2-¹⁸F)fluorotyrosine (F-Tyr) is a promising tracer of protein synthesis (8), since, as evaluated in mice, this compound penetrates easily into the brain, while its metabolites do not cross the blood-brain barrier and no further metabolites are found in the brain tissue. These advantages are combined with the rather long half-life of the label, which permits following tracer uptake into the tissue until accumulation in tissue becomes linear in a Gjedde/Patlak plot. It has also been shown that F-Tyr unlike other halogenated amino acids is almost quantitatively incorporated into proteins (8). Recent biochemical studies with (1-¹⁴C)-tyrosine (9) showed almost identical uptake and metabolic behavior as F-Tyr. Despite the fact that the relative affinities of F-Tyr to carrier enzymes and t-RNA have not been determined, it seemed justified to evaluate F-Tyr in patients with brain tumors of different malignancies. For that purpose, uptake kinetics for F-Tyr in a two- and a three-tissue compartment model were compared to kinetic constants and metabolic rates of glucose as measured by 2(¹⁸F)fluoro-2-deoxy-D-glucose (FDG) and to tracer transport in relation to damage of the blood-brain barrier assessed by ⁶⁸Ga-ethylenediaminetetraacetic acid (EDTA).

MATERIALS AND METHODS

Patient Population

We studied 15 patients, 12 men and 3 women, with mean age 50.6 ± 9.8 (s.d.) yr (Table 1). Five patients had low-grade gliomas, which were classified histologically as astrocytoma of Grade 2 in three cases, whereas the other two were diagnosed clinically and had focal hypodense lesions without contrast enhancement on CT scans. Two patients had histologically proven anaplastic

Received Jul. 17, 1990; revision accepted Jan. 11, 1991.
For reprints contact: W.-D. Heiss, MD, Max-Planck-Institut für neurologische Forschung, Gleueler Str. 50, D-5000 Köln 41, Germany.

TABLE 1
Pertinent Patient Data and Principal Results

Patient	Age (yr)	Sex	Grade	Histology	Previous therapy	$K_1(\text{FDG})^*$	$K_{MR}(\text{FDG})^*$	$K_1(\text{tyr})^*$	$K_{MR}(\text{tyr})^*$	$K_1(\text{Ga})^*$
HE	51	f	2	astrocytoma	surgery	1.25	1.23	2.73	1.65	n.a.
IR	49	m	2	astrocytoma	^{125}I implant.	1.39	1.53	4.62	1.26	5.00
KA	51	m	2	n.a.	none	0.58	0.47	0.96	0.95	0.48
PR	60	m	2	n.a.	none	1.05	0.63	2.91	1.25	0.50
ZI	31	m	2	astrocytoma	none	1.16	1.00	0.75	1.03	n.a.
KO	49	m	3	oligo-astrocytoma	none	1.07	1.18	2.80	1.13	4.00
SN	50	f	3	oligo-astrocytoma	surg., rad., ch.	1.13	1.91	2.96	2.39	4.13
FI	47	m	4	glioblastoma	none	0.90	0.82	2.27	0.38	0.44
HW	57	m	4	glioblastoma	none	0.91	1.13	2.41	1.47	4.80
PF	53	m	4	glioblastoma	none	1.01	1.06	2.91	1.73	29.0
PO	45	f	4	glioblastoma	surg., rad., ch.	0.91	0.93	2.73	1.63	14.0
WN	65	m	4	n.a.	rad. ch.	0.60	0.64	1.21	1.10	n.a.
WR	51	m	4	glioblastoma	surg., rad., ch.	0.57	0.55	1.25	1.14	21.0
BE	33	m	4	gliomatosis	none	0.89	0.68	0.78	0.83	n.a.
LO	67	m		lymphoma	none	1.44	2.69	2.21	0.78	n.a.

Surg. = surgery; rad. = radiation therapy; ch. = chemotherapy; and n.a. = not available.
* All values are given as ratios of tumor-to-contralateral brain.

oligoastrocytomas (WHO-Grade III). Six patients suffered from glioblastomas, of which five were histologically proven. Two additional patients did not fit into those groups: a 67-yr-old man had a cerebral lymphoma, and a 33-yr-old man had diffuse gliomatosis of the frontal lobe. In both cases, diagnosis was based on brain biopsy.

All patients were studied with FDG and F-Tyr, also with ^{68}Ga -EDTA in 11 cases, usually within three consecutive days. In no case was there any substantial therapeutic intervention, such as surgery, radiotherapy, or chemotherapy between scans. Five patients had not received any treatment prior to scanning, apart from corticosteroids or antiepileptic drugs, and four patients had stereotactic tumor biopsy only. One patient with an astrocytoma underwent incomplete tumor resection 3 mo before the PET studies with no other treatment. The remaining five patients suffered from recurring tumors and were examined after previous surgery, radiotherapy, or chemotherapy. In all cases, CT scans showed clear evidence of a solid tumor mass.

Mathematical Model and Model Analysis

In mouse experiments, Coenen et al. (8) demonstrated that F-Tyr is distributed almost exclusively in two compartments of the brain, namely as free F-Tyr in tissue and as a protein bound fraction. From this simple metabolism a two-tissue compartment model, as shown in Figure 1, was proposed. This model is very similar to the deoxyglucose-(DG)-model of Sokoloff et al. (10): free F-Tyr is transported from the cerebral blood pool into brain tissue where it is either incorporated into protein or transported back to blood. The mathematical form of the model equations is identical to the DG-model equations (10) (see Appendix).

The mice data could not provide any information as to the necessity to divide the tissue precursor pool into an extracellular and an intracellular space as shown in Figure 1. However, a significant improvement in the goodness of fit of the model

equations to the PET time activity data may be an indication for the more refined model.

In the fits of the model equations to the PET data, the contribution of plasma activity to total measured activity in a region was taken into account as an additional fit parameter by setting:

$$\text{PET}_i(t) = (1 - \text{CPV}_i) C_i^*(t) + \text{CPV}_i C_p^*, \text{total}(t), \quad \text{Eq. 1}$$

where $\text{PET}_i(t)$ is the time-activity data in region i , $C_i^*(t)$ is the tissue activity as described in Equation A1 or A2 in the appendix, CPV_i is the distribution volume of intravascular plasma activity in that region, and $C_p^*, \text{total}(t)$ total ^{18}F -activity in blood plasma.

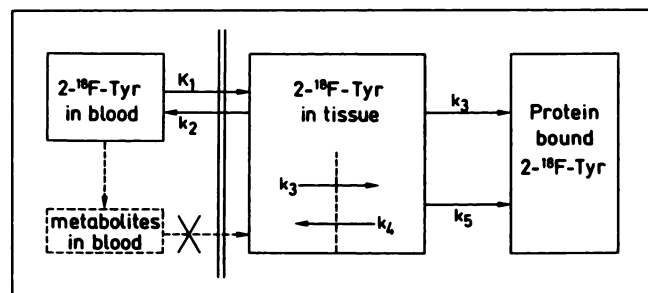


FIGURE 1. Compartment model for $2\text{-}^{18}\text{F}$ -tyrosine uptake with three or five rate constants. K_1 and k_2 refer to forward and reverse transport of F-Tyr across the blood-brain barrier, respectively. In the upper part, k_3 is the rate constant for incorporation into proteins. In the lower part, the three rate constant model is extended to a five-parameter model by adding a further serial tissue compartment with inward and outward transport rate constants k_3 and k_4 , respectively; the incorporation into proteins is then described by rate constant k_5 . It is assumed that metabolites in blood do not cross the blood-brain barrier and that no further metabolites exist in tissue.

The FDG time-activity data were fitted to the Sokoloff DG-model with three rate constants that included the local plasma volume as shown in Equation 1. For calculation of metabolic rate, a lumped constant of 0.42 was used (11). The ^{68}Ga -EDTA data were fitted with a one-tissue compartment model with two rate constants (setting k_3 and k_4 equal to zero in Equation A1) and the plasma volume contribution as a third parameter.

In addition to regional fits of tissue time-activity data with the model equations, parametric images of local plasma volume, accumulation rate, transport, and incorporation rate constants were generated by weighted nonlinear least-squares fits on a pixel-by-pixel basis (12).

Tracer Preparation

L-(2- ^{18}F)fluorotyrosine was prepared by electrophilic radiofluorination of 0-acetyltyrosine as previously described in detail by Coenen et al. (13). Isolation of the product was done by preparative reversed-phase chromatography (Multospher C-18 column, 5 μm , 500 \times 20 mm, eluant: H_2O : acetic acid: methanol: NaCl 95:3:2:0.1 (v,v,v,g) 16 ml/min at 195 bar). Radiochemical purity of the product was checked for each preparation before application to patients by ion-pair HPLC (Nucleosil RP-18 column, 3 μm , 125 \times 4 mm, eluant: Na-citrate HCl buffer, pH 2.7: 1-propanol: Na-dedecylhydrogensulfate 90:10:0.1 (v,v,g) 1 ml/min at 200 bar). The product was chemically and radiochemically pure ($\geq 97\%$) with a specific activity of about 20 GBq/mmol.

FDG was synthesized according to Ehrenkaufner et al. (14). Gallium-68 was applied as ^{68}Ga -EDTA, eluted from a commercially available $^{68}\text{Ge}/^{68}\text{Ga}$ generator. Between 150–200 MBq of the tracers were administered in 3–5-ml pyrogen-free saline solutions as a rapid intravenous bolus.

PET Measurements

The PET measurements with F-Tyr, FDG, and Ga-EDTA were performed on consecutive days. For that purpose, the patients' positions in the gantry were carefully marked on their face and head relative to crossed laser beams. These individual markers allowed for accurate slice repositioning for the following investigations. The standard procedure established in our laboratory for several years (15) was then applied. Data recording was started with injection of the tracer. Seven equally spaced and parallel planes, centered from the canthomeatal line to 81 mm above, were simultaneously scanned for 120 min with F-Tyr, for 40 min with FDG, and for 30 min with Ga-EDTA. The consecutive scan time-intervals were gradually increased from 1 to 5 min. The four-ring positron camera (Scanditronix PC 384-7B) with a spatial resolution of approximately 8 mm FWHM in 11-mm slices (16) gave with this procedure dynamic information about tracer accumulation in virtually all major structures of the brain. About 25 arterialized venous blood samples were obtained manually during the whole scan time, at intervals gradually increasing from 15 sec to 20 min. The degree of arterialization of the venous blood was controlled by measuring P_{O_2} . The blood samples were centrifuged, the plasma activity concentration was measured in a cross-calibrated well counter, and for F-Tyr the percentage of unmetabolized ligand in plasma was determined by HPLC (RP-18 column, 250 \times 4 mm; 2% acetic acid as eluant). Data from the tomographic device and from the sample changer used for plasma counting as well as plasma glucose values determined in duplicate by a standard enzymatic method were stored in the memory of a VAX 11/780 (Digital) computer for later processing.

For all patients, CT scans of the brain with and without contrast agent were available. On the reconstructed PET images, circular or rim shaped regions of interest (ROI) were defined manually on grounds of the corresponding CT scans. The solid tumor mass was outlined, areas of presumed edema or necrosis were not included. A reference region of the same shape and size was placed symmetrically in contralateral brain. The time course of tissue activity in these ROIs was sampled and fitted to the model equations (see Appendix) using an advanced fitting routine (17). The best fits were determined by minimizing a chi square function with respect to variations in the model parameters. Weighting factors that corresponded to the inverse of the variance of regional activity were assigned to each data point. The simplex algorithm (18) and subsequently the variable metric method of Fletcher (19) were used as optimization techniques. The simplex method of Nelder and Mead (18) is rather insensitive to local minima, statistical and rounding errors. Furthermore, it is reasonably fast when far from minimum. The variable metric method of Fletcher (19) is very fast near a minimum, but slower in a nonquadratic region.

RESULTS

F-Tyr Accumulation

Figure 2 shows the time course of unmetabolized F-Tyr activity in blood plasma of one patient study after intravenous injection. Also shown is the progressive increase in F-Tyr metabolites, presented as percent of the total blood plasma activity in three different patient studies. It is evident from this figure that F-Tyr activity in blood plasma decreased rapidly and that F-Tyr is immediately metabolized in the body. After 1 hr, about 50% of the blood activity represents labeled metabolites, at 2 hr after injection metabolite portions over 90% were observed in some cases. The major part of the metabolites was F-Tyr incorporated into proteins as determined by TCA precipitation. Because of the large variations, no attempt was made to extract an average distribution curve from the individual data.

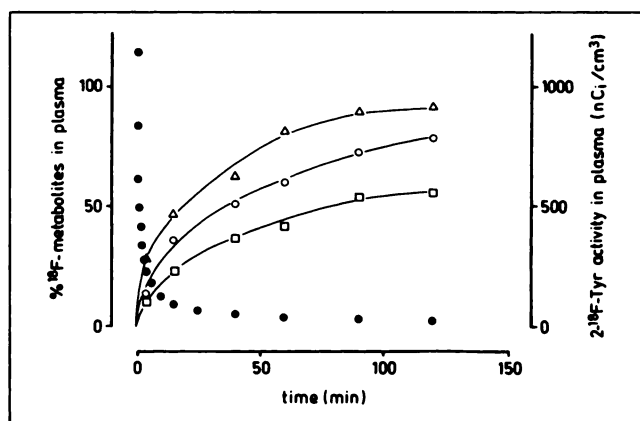


FIGURE 2. Time course of unmetabolized F-Tyr activity and labeled metabolites in blood plasma. Open symbols represent the increase of labeled F-Tyr metabolites in blood plasma as percentage of total plasma activity in three different patient studies. Full dots show the time course of HPLC-measured unmetabolized F-Tyr activity in plasma of one patient study.

TABLE 2
Comparison of F-Tyr Rate Constants Obtained with Three- and Five-Rate Constant Model

Parameter	Tumor		Contralateral Brain	
	3 r.c.	5 r.c.	3 r.c.	5 r.c.
K_1	0.090 ± 0.040	0.117 ± 0.057	0.045 ± 0.016	0.057 ± 0.020
k_2	0.069 ± 0.014	0.138 ± 0.039	0.065 ± 0.020	0.161 ± 0.079
k_3	0.006 ± 0.002	0.052 ± 0.025	0.009 ± 0.004	0.092 ± 0.056
k_4		0.047 ± 0.012		0.070 ± 0.057
k_5		0.008 ± 0.003		0.014 ± 0.008
K_{MR}	0.0064 ± 0.0037	0.0056 ± 0.0035	0.0050 ± 0.0018	0.0044 ± 0.0016

All differences between corresponding values are significant ($p < 0.05$) in Wilcoxon's signed rank test.

The time course of tissue activity data of F-Tyr showed a rapid uptake during the first 5–10 min followed by a continuous efflux over the study interval of 2 hr. The difference between pathologic and normal tissue was much bigger in the early part of the uptake curves with a factor of four between the maxima of tissue activity compared to two-fold higher values at the end of the study after 2 hr. These differences are typical for malignant tumors and the detailed compartmental model analysis will show that there is a striking distinction in the transport from blood into tissue for tumors.

A three-rate constant, two-tissue compartment model, similar to the Sokoloff FDG model with k_3 describing the irreversible incorporation of the tracer, gave generally good fits to the data. However, in several tumor regions, especially those with high fit values for K_1 , the three-rate constant model gave only poor fits to the data especially for the first 20 min of the time-activity curves. The addition of a third tissue compartment resulting in a five-rate constant model improved the unsatisfactory fits significantly. For normal tissue, the five-rate constant model gave only insignificantly better fits than the three-rate constant model in most cases. The F-test (20) was used to check whether improvement in the fit from the three-rate constant to the five-rate constant model was significantly better. For the tumor data in all but three patients, a significantly ($p < 0.05$) better fit was obtained compared to only five patients where the fit to the contralateral time-activity curves also improved.

Fitted rate constants are given in Table 1 and a comparison of the two models for F-Tyr is shown in Table 2. Direct comparison is only possible for K_1 and K_{MR} . K_1 is on average 25% lower in the three-rate constant model than in the five-rate constant model, while K_{MR} is 20% higher. Despite these differences the general results remain stable. In particular a close correlation between K_1 ($r = 0.98$) and K_{MR} ($r = 0.98$), respectively, as calculated from the two models was obtained indicating the robustness of the approach, irrespective of details of the model configuration. Both models and the accumulation curves demonstrate that the main difference between normal and tumorous tissue is the transport rate constant of F-Tyr

from plasma to tissue, K_1 , which is significantly increased in tumors and clearly separates normal from pathologic tissue. Since this rests only on the few cases of this study, further investigations will be needed to confirm this observation. No separation between high- and low-grade lesions was found in the K_1 values.

The rate constant describing the irreversible step of F-Tyr incorporation, k_3 or k_5 , respectively, is in the normal range or even slightly reduced in tumors. Due to the high K_1 values, the accumulation rate, K_{MR} , is increased in tumors with a relationship to the malignancy separating low-grade from high-grade gliomas.

Comparison of F-Tyr with FDG and ^{68}Ga -EDTA

Figure 3 shows matched PET images from a ^{68}Ga -EDTA, a F-Tyr, and a FDG study of a patient with a low-

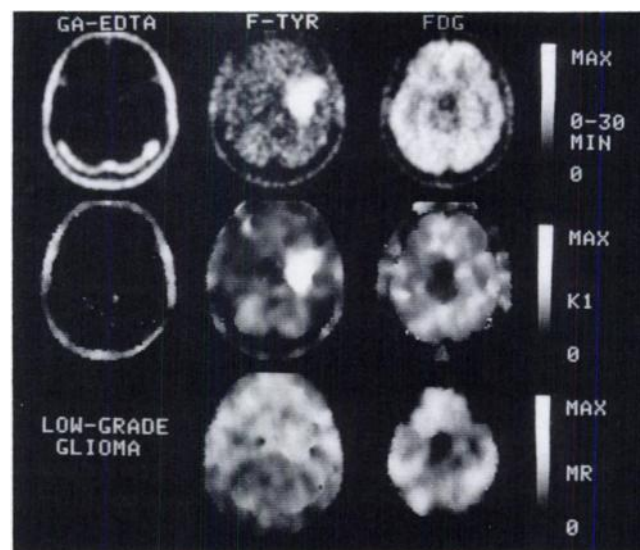


FIGURE 3. Comparison between a ^{68}Ga -EDTA, a F-Tyr and a FDG study of a patient with a low-grade glioma. Upper row: activity images summed over 30 minutes after injection of 185 MBq. Middle row: functional images of the transport rate constant K_1 . The MAX values are $0.05 \text{ ml g}^{-1}\text{min}^{-1}$ for ^{68}Ga -EDTA and $0.15 \text{ ml g}^{-1}\text{min}^{-1}$ for F-Tyr and FDG. Lower row: accumulation rate K_{MR} for F-Tyr and FDG. The MAX values are $0.012 \text{ ml g}^{-1}\text{min}^{-1}$ for F-Tyr and $50 \mu\text{mole glucose (100 g)}^{-1}\text{min}^{-1}$ for FDG.

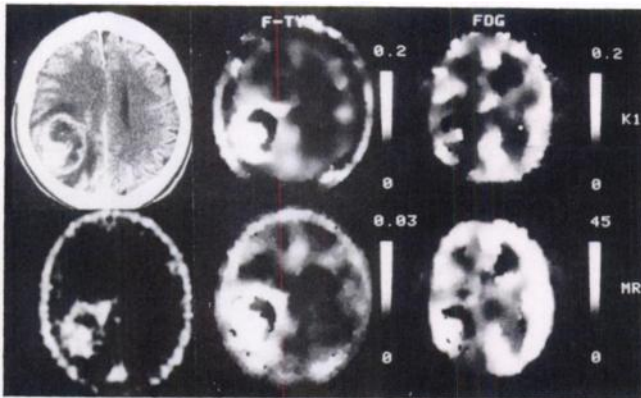


FIGURE 4. Comparison between CT, ^{68}Ga -EDTA accumulation, and functional images of the transport rate constant K_1 and of the accumulation rate K_{MR} for F-Tyr and FDG of a patient with a glioblastoma.

grade glioma. The upper three images represent activity data summed over the first 30 min after bolus injection of the respective tracer. Functional images also are shown of the transport rate constant K_1 as well as the F-Tyr and FDG accumulation rates, K_{MR} , as determined from pixel-by-pixel fits of the whole time sequence of the tissue uptake data. The extension of the tumor was clearly visible only in the F-Tyr images, mainly in the activity and K_1 representations. The FDG study showed a reduced glucose consumption in the tumor area, and in the ^{68}Ga -EDTA images no damage of the blood-brain barrier was indicated. A somewhat different feature showed the comparative study of a glioblastoma (Fig. 4). Again, as in most instances, the extension of the tumor was best demarcated on the F-Tyr image, while the FDG scan separates the solid tumor rim and the necrotic core with low metabolism. In summary, increased ^{68}Ga -EDTA uptake was preferentially seen in tumor areas with contrast enhancement on x-ray CT, such as the rim around the central necrosis of the glioblastoma, but it also appeared in tumor core regions probably housing necrosis from CT appearance and low metabolic activity. In contrast, increased F-Tyr

together with increased FDG accumulation was usually located in solid, probably actively proliferating tumor parts; their uptake was below normal in necrotic tissue.

Gjedde/Patlak plots (21) of the three tracers in normal and tumorous tissue of the patient presented in Figure 4 are shown in Figure 5. In tumors, F-Tyr and ^{68}Ga -EDTA activity show a fast initial rise related to increased blood-tissue penetration; the accumulation rate reaches zero for ^{68}Ga -EDTA after this initial slope. For FDG, tracer uptake in tumor tissue continues to rise after the initial extraction, indicating increased irreversible metabolic turnover. The Gjedde/Patlak plots characterize the differences of tumor-to-normal tissue. Gallium-68-EDTA indicates a parallel shift of the activity after the increased initial diffusion. For F-Tyr, the curves are separated in the initial slopes indicating increased transport in tumors; these curves have similar slopes later due to comparable incorporation rates. FDG curves diverge progressively due to the different phosphorylation rates in tumor and normal tissue. Average values of the kinetic constants (K_1 , k_2 , k_3) fitted to the accumulation of the metabolic rate (K_{MR}) and of the distribution volume of the non-metabolized tracer ($V_d = K_1/(k_2 + k_3)$) for all patients irrespective of tumor type are listed in Table 3. Significantly higher values in tumor than in contralateral cortex were found for blood-to-tissue transport and distribution volume of F-Tyr and ^{68}Ga -EDTA, whereas k_3 of F-Tyr was slightly lower in tumors than in contralateral cortex. FDG did not show any significant global differences between tumor and contralateral cortex in the averaged values.

Since rate constants of processes mediated by carriers or enzymes and derived accumulation rates depend on the level of competing substances, which may vary between subjects, all values were related to contralateral unaffected cortex and tumor-to-normal tissue ratios were used for comparison between tracers. Correlations between tumor grade and these ratios were found for ^{68}Ga -EDTA and FDG: blood-to-tissue transport rates and distribution volumes, relative to contralateral cortex, increased for ^{68}Ga -EDTA from 1.98 ± 2.61 (K_1 -ratio) and 0.68 ± 0.20 (V_d -

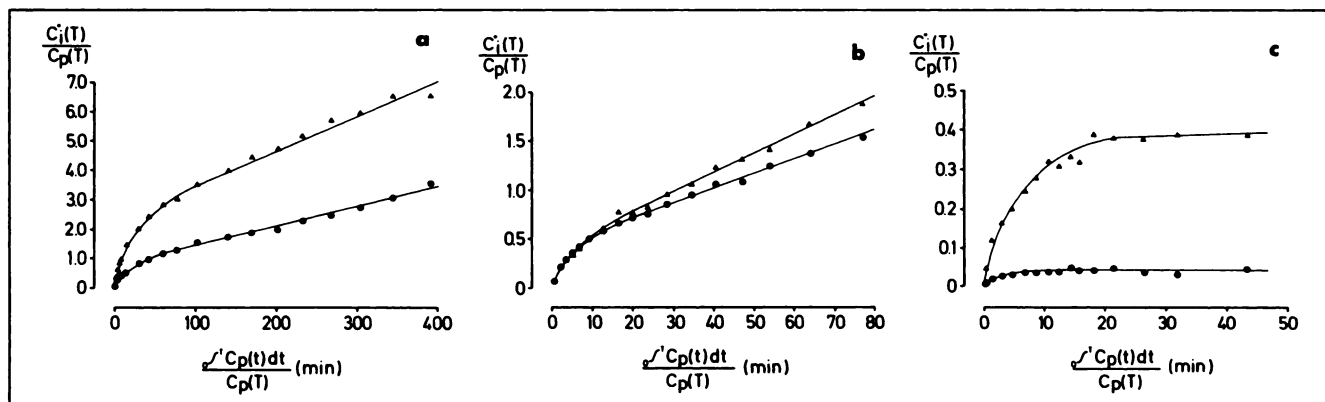


FIGURE 5. Gjedde/Patlak plots of F-Tyr (A), FDG (B), and ^{68}Ga -EDTA (C) accumulation in a glioblastoma (open triangles) and contralateral normal tissue (full circles). The solid curves are model fits to the data.

TABLE 3
Average Rate Constants and Distribution Volumes in All Patients (mean \pm s.d.)

Parameter	Tracer	Tumor	Contralat. Cortex	p*
K_1 (ml/g/min)	F-Tyr	0.090 \pm 0.040	0.045 \pm 0.016	0.003
	FDG	0.084 \pm 0.021	0.086 \pm 0.012	n.s.
	$^{68}\text{Ga-EDTA}$	0.015 \pm 0.012	0.004 \pm 0.004	0.047
k_2 (min^{-1})	F-Tyr	0.069 \pm 0.014	0.065 \pm 0.020	n.s.
	FDG	0.168 \pm 0.041	0.170 \pm 0.032	n.s.
	$^{68}\text{Ga-EDTA}$	0.152 \pm 0.091	0.266 \pm 0.395	n.s.
k_3 (min^{-1})	F-Tyr	0.006 \pm 0.002	0.009 \pm 0.004	0.004
	FDG	0.058 \pm 0.031	0.051 \pm 0.017	n.s.
K_{MR} (ml/g/min)	F-Tyr	0.006 \pm 0.004	0.005 \pm 0.002	n.s.
	FDG	0.020 \pm 0.007	0.020 \pm 0.005	n.s.
V_d (ml/g)	F-Tyr	1.270 \pm 0.616	0.619 \pm 0.177	0.002
	FDG	0.384 \pm 0.103	0.394 \pm 0.055	n.s.
	$^{68}\text{Ga-EDTA}$	0.128 \pm 0.107	0.024 \pm 0.017	0.028

* Significance probability for difference between tumor and contralateral cortex in Wilcoxon test.

F-Tyr values are from the three-rate constant-model.

ratio) in low-grade gliomas to 13.84 ± 11.64 and 14.49 ± 11.12 , respectively, in glioblastomas, whereas the corresponding FDG values decreased slightly with increasing malignancy (K_1 -ratio: 1.09 ± 0.31 in low-grade gliomas versus 0.82 ± 0.18 in glioblastomas; V_d -ratio: 1.22 ± 0.15 versus 0.80 ± 0.13). In contrast to these relations, which yielded significant Kendall rank correlation coefficients with tumor grade, no consistent relation between F-Tyr transport (K_1) and tumors grade was observed, and increased transport of F-Tyr was seen in most tumors irrespective of their grade.

There was no correlation of influx rate constants (K_1) between F-Tyr and $^{68}\text{Ga-EDTA}$ ($r = 0.06$), but a loose, still significant correlation ($r = 0.61$, $p < 0.02$) was observed between K_1 of F-Tyr and FDG. Thus, influx of the two low-molecular weight substances with carrier-mediated transport was apparently more closely related than either with the passive blood-brain barrier damage indicator $^{68}\text{Ga-EDTA}$, which is a much larger molecule. Correlations of tissue-to-blood transport rate constants (k_2) and metabolic rate constants (k_3) were small and not significant for F-Tyr and FDG.

DISCUSSION

Kinetic Analysis and Transport

The kinetic analysis of F-Tyr uptake in comparison to glucose metabolism and $^{68}\text{Ga-EDTA}$ uptake clearly demonstrates that the increased tracer accumulation in tumors is mainly due to the increased transport (K_1) of amino acids into the tissue and not due to increased irreversible incorporation into proteins (k_3 or k_5). In contrast, increase in glucose consumption observed in most gliomas (22,23) are mainly due to an altered glucose phosphorylation

expressed by k_3 in the three-compartment model (24). Local changes in F-Tyr accumulation are not correlated to a disruption of the blood-brain barrier as investigated by $^{68}\text{Ga-EDTA}$. While in our small sample F-Tyr uptake was not highly correlated to tumor grade—as has been reported in larger series for ^{11}C -methyl-methionine (3,25), the increased transport rate constants of F-Tyr permitted a sharp distinction between normal and tumorous tissue yielding an important criterion especially for differentiation between low-grade gliomas and other tissue in addition to FDG studies, which are better suited to differentiate between tumor grades (22). For this purpose, F-Tyr might be of clinical value since low-grade gliomas can hardly be distinguished from normal tissue or from vascular lesions by their FDG or $^{68}\text{Ga-EDTA}$ uptake.

In normal brain tissue, the sodium-independent bidirectional L-system is the predominant carrier of large neutral amino acids including tyrosine and probably fluorotyrosine (26–29). Since in brain tumors, uptake of both, L- and D-methionine (30) is increased, a change in transport mechanisms must be postulated, because binding to the carriers is less specific than t-RNA mediated incorporation into proteins. This incorporation rate, which is described by k_3 or k_5 , was not altered, whereas the total accumulation rate (K_{MR}) was increased in tumors due to the effect of altered K_1 .

While passive diffusion does not contribute significantly to the penetration of amino acids into brain cells, the gradual disruption of the blood-brain barrier with progressively malignancy of tumors could affect amino acid uptake: the blood-brain barrier may become permeable for relatively small molecules like F-Tyr and FDG in low-grade tumors, and progressively also for larger molecules like $^{68}\text{Ga-EDTA}$ in more malignant tumors. However, our

data did not indicate proportional changes of FDG and F-Tyr transport and relation to the high ^{68}Ga -EDTA uptake in more malignant tumors. Additional evidence against passive diffusion of F-Tyr across a damaged blood-brain barrier can be seen in the increase of V_d above 1 ml/g (mean 1.270 ± 0.615). Such an effect could be caused by activation of amino acid transport system A. It is Na^+ -dependent, has been located asymmetrically at the abluminal side of the blood-brain barrier (31), and may be activated in tumor cells (28).

Model for Determination of Protein Synthesis

Tissue time-activity data as measured by PET generally show a rather smooth curve that can easily be characterized by a small number of parameters. For practical purposes, the model used to describe complex biochemical processes therefore can be rather simple. The validity of the model and of its assumptions must be tested by its capability to describe the data and by additional information about various metabolic pathways that often can only be determined in animal experiments. In the studies of F-Tyr in mice brains by Coenen et al. (8), it was shown that the incorporation of this amino acid into cerebral proteins is fast and that ^{18}F activity in cerebral tissue is distributed almost exclusively into two pools that are the protein-formed fraction and free F-Tyr. Based on these data, a two-tissue compartment model was used that adequately described the F-Tyr accumulation in normal tissue, but only unsatisfactorily fitted the data in tumorous tissue. In order to improve the fit of the calculated curves to the actual activities, an additional third tissue compartment was introduced into the model. The physiologic meaning of this additional compartment remains unclear, since the improvement of the mathematical fit to the data is no proof of the physical presence of such a compartment. The large heterogeneity of tissue compartments in tumors characteristic for high-grade gliomas (32) and the limited spatial resolution of the PET method could cause inadequate fits in a three-rate constant model that will always be improved by addition of further parameters. However, in tumors other processes also could represent additional metabolic compartments as reversible binding of the tracer to special enzymes, abnormal proteins or pathways different from normal tissue. These questions cannot be answered by the mathematical analysis of PET data but require extensive *in vitro* investigations of tumor metabolism.

As demonstrated by stimulation procedures (33), any two- or three-tissue compartment model with a final irreversible step tends to overestimate metabolism in inhomogeneous tissue, since all slow processes without significant backflux during the observation period will be covered within the unidirectional metabolic step. Therefore, the absence of an increase in that step—in our data of F-Tyr incorporation into proteins—is a more reliable finding than the opposite would have been.

F-Tyr permits prolonged recordings sufficient to determine both the transport into tissue and the incorporation into proteins accurately. Quantification of absolute rates of protein synthesis with F-Tyr is currently precluded by insufficient knowledge about the intracellular level of competing amino acids, which may originate from plasma, from other metabolic pathways and from protein degradation (34,35). In addition, the lumped constant accounting for differences between natural tyrosine and F-Tyr in the relative affinities to carrier enzymes and to t-RNA is not known. However, comparison with (1- ^{14}C)-tyrosine indicates a similar behavior (9). Therefore, evaluation of F-Tyr accumulation is currently limited to comparison with contralateral unaffected tissue. Despite the limitations inherent in all approaches to quantitation of protein synthesis in man today, F-Tyr has several properties suggesting its application as a PET tracer for protein synthesis in the brain:

1. It can be reproducibly synthesized.
2. It has a high blood-brain barrier permeability.
3. No labeled metabolites cross the blood-brain barrier.
4. No metabolites are formed in brain tissue except tracer amounts of (6- ^{18}F)dopamine in the striatal area (36).
5. Its unidirectional uptake into brain tissue leads to accumulation characteristics approaching linearity asymptotically.
6. The long half-life of the ^{18}F label permits following of tracer uptake for sufficient time periods.

When plasma activity is determined and corrected for labeled metabolites, as done in our study, the quantification of accumulation kinetics—transport and irreversible incorporation—can be expected to be more accurate than in previous studies employing ^{11}C -methionine or its methyl or S-adenosyl-derivatives (37), since the metabolic pathways of F-Tyr are less complex than those of methionine (8). For methionine and its derivatives, the significant portion of metabolic pathways other than incorporation into proteins limited its use for quantitative analysis of protein synthesis. The less complex metabolism of F-Tyr suggestive of unidirectional kinetics indicates the potential of this compound as a tracer for protein synthesis. However, before a quantitative model similar to that for determination of glucose metabolism with FDG can be established, further experiments are needed to determine all the interrelated variables of the kinetic model and their alterations in pathology.

APPENDIX

For the three-rate constant model (see Fig. 1), the time course of the tissue activity is given by:

$$C_i^*(t) = K_1 \left[\frac{k_3}{k_2 + k_3} \int_0^t C_p^*(t') dt' + \frac{k_2}{k_2 + k_3} \exp[-(k_2 + k_3)t] \cdot \int_0^t C_p^*(t') \exp[(k_2 + k_3)t'] dt' \right] \quad \text{Eq. A1}$$

The accumulation rate K_{MR} is then expressed by $K_1 k_3 / k_2 + k_3$.

From the differential equations for the three-tissue compartment-five-rate constant model in Figure 1, the time dependence of the total tissue activity as measured by PET can be derived as:

$$C_i^*(t) = \frac{K_1}{\alpha_1 - \alpha_2} \left[\left(\alpha_1 + k_3 + k_4 + k_5 + \frac{k_3 k_5}{\alpha_1} \right) e^{\alpha_1 t} - \left(\alpha_2 + k_3 + k_4 + k_5 + \frac{k_3 k_5}{\alpha_2} \right) e^{\alpha_2 t} \right] \oplus C_p^*(t) + \frac{K_1 k_3 k_5}{k_2 k_4 + k_2 k_5 + k_3 k_5} \int_0^t C_p^*(t') dt', \quad \text{Eq. A2}$$

where $C_i^*(t)$ is the total ^{18}F -Tyr activity in tissue, \oplus denotes the operation of convolution, and

$$\alpha_1 = -\frac{k_2 + k_3 + k_4 + k_5}{2} - \frac{1}{2} \sqrt{(k_2 + k_3 + k_4 + k_5)^2 - 4(k_2 k_4 + k_2 k_5 + k_3 k_5)}$$

$$\alpha_2 = -\frac{k_2 + k_3 + k_4 + k_5}{2} + \frac{1}{2} \sqrt{(k_2 + k_3 + k_4 + k_5)^2 - 4(k_2 k_4 + k_2 k_5 + k_3 k_5)}$$

The accumulation rate in this case is given by:

$$K_{MR} = \frac{K_1 k_3 k_5}{k_2 k_4 + k_2 k_5 + k_3 k_5},$$

where $C_p^*(t)$ is the plasma activity corrected for metabolites, thus representing the concentration of F-Tyr in plasma.

REFERENCES

- Siegel GJ, Albers RW, Agranoff BW, Katzman R. *Basic neurochemistry*, third edition. Little, Brown and Company; Boston: 1981.
- Bustany P, Chatel M, Derlon JM, Sgouropoulos P, Soussaline F, Syrota A. Brain tumor protein synthesis and histological grades: a study by positron emission tomography (PET) with C-11-L-methionine. *J Neuro-Oncol* 1986;3:397-404.
- Schober O, Meyer GJ, Gaab MR, Müller JA, Hundeshagen H. Grading of brain tumors by C-11-L-methionine PET. *J Nucl Med* 1986;27:890-891.
- Bolster JM, Vaalburg W, Paans AMJ, et al. Carbon-11-labelled tyrosine to study tumor metabolism by positron emission tomography (PET). *Eur J Nucl Med* 1986;12:321-324.
- LaFrance ND, O'Tuama L, Villemagne V, et al. Quantitative imaging and follow-up experience of C-11-L-methionine accumulation in brain tumors with positron emission tomography. *J Nucl Med* 1987;28:645.
- Ericson K, Blomqvist G, Bergström M, Eriksson L, Stone Elander S. Application of a kinetic model on the methionine accumulation in intracranial tumors studied with positron emission tomography. *Acta Radiol* 1987;28:505-509.
- Hawkins RA, Huang SC, Barrio JC, et al. Estimation of local cerebral protein synthesis rates with L-(1- ^{11}C)Leucine and PET: methods, model, and results in animals and humans. *J Cereb Blood Flow Metab* 1989;9:446-460.
- Coenen HH, Kling P, Stöcklin G. Cerebral metabolism of L-(2- ^{18}F)fluorotyrosine, a new PET tracer or protein synthesis. *J Nucl Med* 1989;30:1367-1372.
- Ishiwata K, Vaalburg W, Elsinga PH, Paans AMJ, Woldring MG. Metabolic studies with L(1- ^{14}C) tyrosine for the investigation of a kinetic model to measure protein synthesis rates with PET. *J Nucl Med* 1988;29:524-529.
- Sokoloff L, Reivich M, Kennedy C, et al. The (^{14}C)deoxyglucose method for the measurement of local cerebral glucose utilization: theory, procedure, and normal values in the conscious and anesthetized albino rat. *J Neurochem* 1977;28:897-916.
- Phelps ME, Huang SC, Hoffman EJ, Selin C, Sokoloff L, Kuhl DE. Tomographic measurement of local cerebral glucose metabolic rate in humans with (F-18)2-fluoro-2-deoxy-D-glucose: validation of method. *Ann Neurol* 1979;6:371-388.
- Herholz K. Non-stationary spatial filtering and accelerated curve fitting for parametric imaging with dynamic PET. *Eur J Nucl Med* 1988;14:477-484.
- Coenen HH, Franken K, Kling P, Stöcklin G. Direct electrophilic radiofluorination of phenylalanine, tyrosine and dopa. *Appl Radiat Isot* 1988;39:1243-1250.
- Ehrenkauf RE, Potocki JE, Jewett DM. Simple synthesis of F-18-labeled-2-fluoro-2-deoxy-D-glucose: concise communication. *J Nucl Med* 1984;25:333-337.
- Heiss WD, Pawlik G, Herholz K, Wagner R, Göldner H, Wienhard K. Regional kinetic constants and CMRGlu in normal human volunteers determined by dynamic positron emission tomography of (^{18}F)-2-fluoro-2-deoxy-D-glucose. *J Cereb Blood Flow Metab* 1984;4:212-223.
- Litton J, Bergström M, Eriksson L, Bohm C, Blomqvist G, Kesselberg M. Performance study of the PC-384 positron camera system for the brain. *J Comput Assist Tomogr* 1984;8:74-87.
- James F, Roos M. MINUIT—a system for function minimization and analysis of the parameter errors and correlations. *Comput Phys* 1976;10:343-376.
- Nelder JA, Mead R. A simplex method for function minimization. *Comput J* 1965;7:308.
- Fletcher R. A new approach to variable metric algorithms. *Comput J* 1970;13:317.
- Landaw EM, DiStefano III JJ. Multiexponential, multicompartmental, and noncompartmental modeling. II. Data analysis and statistical considerations. *Am J Physiol* 1984;246:R665-677.
- Patlack CS, Blasberg RG, Fenstermacher JD. Graphical evaluation of blood-to-brain transfer constants from multiple-time uptake data. *J Cereb Blood Flow Metab* 1983;3:1-7.
- DiChiro G. Positron emission tomography using (^{18}F)fluorodeoxyglucose in brain tumors. A powerful diagnostic and prognostic tool. *Invest Radiol* 1986;22:360-371.
- Alavi JB, Alavi A, Chawluk J, et al. Positron emission tomography in patients with glioma. A predictor of prognosis. *Cancer* 1988;62:1074-1078.
- Herholz K, Ziffling P, Staffen W, et al. Uncoupling of hexose transport and phosphorylation in human gliomas demonstrated by PET. *Eur J Cancer Clin Oncol* 1988;24:1139-1150.
- Derlon JM, Bourdet C, Bustany P, et al. (^{11}C)L-methionine uptake in gliomas. *Neurosurgery* 1989;25:720-728.
- Pardridge WM. Brain metabolism: a perspective from the blood-brain barrier. *Phys Rev* 1983;63:1481-1535.
- Audus KL, Borchardt RT. Characteristics of the large neutral amino acid transport system of bovine brain microvessel endothelial cell monolayers. *J Neurochem* 1986;47:484-488.
- Christensen HN. Role of amino acid transport and countertransport in nutrition and metabolism. *Phys Rev* 1990;70:43-77.
- Lajtha A, Toth J. The brain barrier system. V. Stereospecificity of amino acid uptake, exchange, and efflux. *J Neurochem* 1963;10:909-920.
- Schober O, Duden C, Meyer GJ, Müller JA, Hundeshagen H. Nonselective transport of (C-11-methyl)-L- and D-methionine into a malignant glioma. *Eur J Nucl Med* 1987;13:103-105.
- Betz AL, Goldstein GW. Polarity of the blood-brain barrier: neutral amino acid transport into isolated brain capillaries. *Science* 1978;202:225-227.
- Heiss WD, Heindel W, Herholz K, et al. Positron emission tomography of fluorine-18-deoxyglucose and image-guided phosphorus-31 magnetic resonance spectroscopy in brain tumors. *J Nucl Med* 1990;31:302-310.

33. Herholz K, Patlack CS. The influence of tissue heterogeneity on results of fitting nonlinear model equations to regional tracer uptake curves: with an application to compartmental models used in positron emission tomography. *J Cereb Blood Flow Metab* 1987;7:214-229.
34. Phelps ME, Barrio JR, Huang SC, Keen RE, Chugani H, Mazziotta JC. Criteria for the tracer kinetic measurement of cerebral protein synthesis in humans with positron emission tomography. *Ann Neurol* 1984; 15(suppl):S192-S202.
35. Smith CB, Deibler GE, Eng N, Schmidt K, Sokoloff L. Measurement of local cerebral protein synthesis in-vivo: influence of recycling of amino acids derived from protein degradation. *Proc Natl Acad Sci USA* 1988;85:9341-9345.
36. Coenen HH, Wutz W, Stöcklin G, DeGrado T, Kling P. Pharmacokinetics and metabolism of L-(2-¹⁸F) fluorotyrosine in the brain and periphery of mice. *J Nucl Med* 1990;31:786.
37. Ishiwata K, Ido T, Abe Y, Matsuzawa T, Iwata R. Tumor uptake studies of S-adenosyl-L-(methyl-C-11) methionine and L-(methyl-C-11)methionine. *Nucl Med and Biol* 1988;15:123-126.

EDITORIAL

Which PET Radiopharmaceutical for Brain Tumors?

After an initial period of skepticism about the meaning and purpose of PET in the study of brain tumors, we are now observing an explosion of interest in the subject. The message that CT and MR examinations, despite their exquisite anatomical depiction, fail to provide the critically important information necessary for appropriate management of these neoplasms, has pierced through. Twelve years ago, our fledgling PET tumoral research at the National Institutes of Health was labeled by some as "redundant and irrelevant." CT and the just-being-introduced MRI were rendering brain tumor diagnosis a "settled matter."

Yet, today the clinical challenge of handling primary brain tumors remains formidable and controversies abound (1-4). When should we start to use any of the three main therapeutic means available to us, i.e., surgery, radiotherapy, and chemotherapy? In the low-grade gliomas, should we delay surgery and radiotherapy as long as possible? Is open surgery actually necessary in every case of high-grade glioma? How far can we rely on stereotactic sampling? Should we favor stereotactic radiosurgery for suspected high-grade, deep lesions, even in the absence of histologic confirmation? Do CT, MR, or arteriography allow us to grade primary brain tumors? What path should we follow when confronted with renewed clinical de-

terioration after radiotherapy, considering that CT, MR, and arteriography do not allow us to confidently differentiate between tumor recurrence and cerebral radiation necrosis? Should we proceed with additional surgery, interstitial radiotherapy, pass to chemotherapy, or abstain from further treatment? Should we obtain histologic confirmation? Should histology represent the definitive guide at every step of the management? Does, in fact, histology consistently assist us in the prognostic assessment of these patients? Or rather, has the static histologic examination exhausted its role, held since the age of Cruveilhier, Rokitsansky and Virchow, as the ultimate, unappealable test? The list of questions seems inexhaustible.

What is clearly needed is an assessment of the biologic behavior of the tumor, a complex matter, considering that even the frequency of natural change to higher malignancy of low-grade neoplasms remains controversial (2,3). Use of radiotracers, particularly analogs of physiologic compounds, is considered the tool most likely to assist us in this area. Even in 1961, a report dealing with radioisotope brain imaging (5) noted that: "The degree of differentiation of a tumoral lesion is important in determining the uptake ratio. Tumors of the glioblastoma group show a high ratio. On the other hand relatively benign and well differentiated tumors, such as some astrocytomas, present the lowest concentration of isotope."

When, in 1979, the seminal contribution by Reivich et al. on PET with ¹⁸F-2-deoxyglucose (FDG) was published (6), it was only obvious that

this tracer, with its capability to measure the degree of cerebral tissue glucose utilization, should be tried for grading brain tumors. The linkage glucose consumption-malignancy had been forcefully proposed by Otto Warburg, who suggested that neoplasms display higher rates of aerobic glycolysis with increasing degree of malignancy (7). (By aerobic glycolysis, Warburg meant the metabolism of glucose to lactate rather than to CO₂ and H₂O, even in the presence of adequate available O₂.) Thus, the already high energy demands of rapidly proliferating tumoral tissue are further increased by the shift toward the less efficient glycolytic pathway. This marriage of a proven radiotracer with a compelling theoretical framework proved successful; PET centers throughout the world now use FDG to study brain tumors, as well as tumors in other parts of the body.

However, studies of neoplasia with PET have not been limited to a single radiopharmaceutical. Besides FDG, other tracers tagged with positron emitters have been suggested, introduced and tested, in mostly smaller and sometimes larger series of patients, to assess the biologic behavior of the tumor. They include other sugars and sugar derivatives, amino acids, nucleosides, putrescine, and receptor ligands labeled with ¹⁸F, ¹¹C, or ¹³N, as well as ¹³N-labeled ammonia. Appropriate radiopharmaceuticals have also been used in tumors for PET studies of disruption of the blood-brain barrier, changes in blood flow, blood volume, pH, and pharmacokinetics of chemotherapeutic drugs. In this issue of the *Journal*, an ¹⁸F-tagged

Received Feb. 20, 1991; revision accepted Feb. 20, 1991.

For reprints contact: Giovanni Di Chiro, MD, Tomography Section, National Institutes of Health, Bldg. 10, Rm. 3010, Bethesda, MD 20205.